Investigation of a Terahertz Antenna for Continuous Wave Nanophotomixer

Untersuchung einer Terahertz-Antenne für Dauerstrich Nanophotomixer

Author:	**Celia Peña Masiá**
Degree Programme:	**Information and Communication Engineering**
Examiner:	**Prof. Dr. Thomas Kusserow**
Department:	**Institute for Microwave Engineering and Photonics**
Supervisor:	**Dr. Ing. Shihab Al-Daffaie**
Start Date:	**23.04.2019**
Date Of Submission:	**22.10.2019**
Examination Date:	
Bachelor thesis	**(2292-B)**

TECHNISCHE UNIVERSITÄT DARMSTADT

Affidavit/Eidesstattliche Versicherung

Erklärung zur Abschlussarbeit gemäß §22 Abs. 7 und §23 Abs. 7 APB TU Darmstadt
Hiermit versichere ich, Celia Peña Masiá, die vorliegende Master-Thesis / Bachelor-Thesis gemäß §22 Abs. 7 APB der TU Darmstadt ohne Hilfe Dritter und nur mit den angegebenen Quellen und Hilfsmitteln angefertigt zu haben. Alle Stellen, die Quellen entnommen wurden, sind als solche kenntlich gemacht worden. Diese Arbeit hat in gleicher oder ähnlicher Form noch keiner Prüfungsbehörde vorgelegen.
Mir ist bekannt, dass im Falle eines Plagiats (§38 Abs.2 APB) ein Täuschungsversuch vorliegt, der dazu führt, dass die Arbeit mit 5,0 bewertet und damit ein Prüfungsversuch verbraucht wird. Abschlussarbeiten dürfen nur einmal wiederholt werden.
Bei der abgegebenen Thesis stimmen die schriftliche und die zur Archivierung eingereichte elektronische Fassung gemäß §23 Abs. 7 APB überein.

Place, Date	Author

Zusammenfassung/Abstract

In dieser Arbeit würden die Möglichkeiten von direkter Adressierung des Impedanz-Fehlanpassungen Problems von dem Dauerstrichbetrieb (CW) Generierung in Terahertz (THz) aus beiden unterschiedlichen Konfigurationen von konventionellen und Nano- Photomixers erforscht. Hier wurden Zwei Antennendesigns untersucht; Breitband und Resonanz Antennen. Eine logarithmisch-periodische Antennendesign wurde für einen breiten Frequenzbereich gewählt, und Vollwellen Dipole für Resonanz Antenne. Es wurden die Möglichkeiten von der Implementierung eines konzentrierten-Element Anpassnetzwerks diskutiert. Die geringe Leistungsübertragung zwischen Photomixer und Antenne fokussiert welche auf klassisch verteilten Matching-Netzen auf Übertragungsleitungen basieren, welche Nicht für diese Anwendung geeignet. Die passenden Elemente werden für beide konventionellen berechnet und Nanophotomischer. Darüber hinaus kann die Verwendung von Nanomaterial als Elektroden die Leistung der photoleitenden Terahertz-Optoelektronik bei niedrigem Quantenwirkungsgrad erheblich verringern. Dies verbessert den Wirkungsgrad der Umwandlung von optischen in Terahertz von photoleitenden Terahertz-Emittern. Zusammenfassend lässt sich sagen, dass diese Studie es ermöglicht, die unterschiedlichen Rollen der Photomixer- und Antennenintegration besser zu verstehen und diese Komponenten daher unabhängig zu optimieren.

This work studies the possibilities of directly addressing the impedance mismatch problem of a continuous wave (CW) terahertz (THz) generation from different both configuration of conventional and nano photomixers. Two antenna designs are investigated here, the broadband and resonance antennas. A log-periodic antenna design is chosen for broad frequency range, and full-wave dipole for resonance antenna. The possibilities of implementing a lumped element matching network are discussed. The values obtained of the matching elements are, for the interdigital photomixer $L = 7.93$ pH and $C = 1.88$ fF, and for the single nanowire $L = 50$ pH and $C = 0.3$ fF. The low power transfer between the photomixer and antenna focuses in which classical distributed matching networks based in transmission lines are not suitable for this application. The matching elements are calculated for both conventional and nano photomixers. Moreover, the use of nanomaterial as electrodes can significantly mitigate the low-quantum efficiency performance of photoconductive terahertz optoelectronics. This enhances the optical-to-terahertz conversion efficiency of photoconductive terahertz emitters. In conclusion, this study allows to understand better the distinct roles of the photomixer and antenna integration and, hence, independently optimize these components.

Contents

1 Introduction

Terahertz (THz) gap is located between microwave and optical regions over the spectrum of electromagnetic waves. In the past, the term of "gap" was used since it had not been possible to bridge the high-frequency limit of RF sources with the low-frequency end of optical emitters. Within the last decade, however, efforts to build suitable sources and detectors have drastically closed the gap.

The THz frequency range has been historically used in excitations of semiconductors and dielectrics [1–5]. However, a wide range of potential applications has been observed. Comparing to microwaves, imaging of macroscopic objects with rather high spatial resolution is possible with THz radiation due to the submillimeter wavelength. On the other hand, this frequency band has also a special importance for spectroscopy in astrophysics [6–8] owing to the fact that many astrophysical objects emit in the THz range of the spectrum. In addition, THz technology is promising for wireless communication systems as a replacement for transmitters and receivers operating in high-frequency and microwave ranges. For this reason, it can potentially increase the speed of data transfer by hundreds of times [9, 10].

Nowadays, the most common method of low power THz generation involves the use of surface conductivity in semiconductor structures [11]. Two or more conductive electrodes spaced by a certain gap are deposited onto semiconductor surface and biased by an external voltage. If the structure is pumped by a femtosecond optical pulse, it is referred to a THz photoconductive antenna. Otherwise, when the excitation comes from a continuous wave (CW) pump by two lasers operating at close wavelengths, whose difference frequency lies in the THz spectral range, is called THz photomixer.

When exciting the gap between the electrodes with a laser, the concentration of charge carriers increases sharply for a short period of time. The photogenerated current, $I(t)$, is fed into a suitably designed antenna. At this point, THz pulse generation occurs. The duration of this pulse and its spectrum are determined mainly by the carriers lifetime in the semiconductor. In the case of CW pumping, carrier concentration changes with difference frequency of pump wavelengths, and CW THz signal is emitted.

This work is focused on the latest developments in CW photomixing for THz generation. A realization for the desired THz frequency is also presented, with a log-periodic planar antenna designed for covering a broad frequency range with constant impedance and farfield pattern. One of the most critical problems in terms of power generation is the mismatching betwenn the low impedance value of the antenna ($\sim 50\ \Omega$) comparing to the high impedance value ($\sim 10k\Omega$) of the photomixer. This leads to high power transfer losses. The photoconductive antenna design has to carefully take into account the antenna impedance, device capacitance and the photoconductance to achieve better performance in terms of higher THz radiation power in broadband devices.

This work focuses on describing the different steps related to terahertz generation. Firstly, two different terahertz antenna are presented followed by terahertz generation by means of photomixing. Moreover, photomixers based in plasmonics are presented, depending on the configuration and material used. Finally, the integration between the antenna and the photomixer is adressed, describing the suitability of matching networks to solve the power transfer problem.

2 THz Antenna

One of the major advantages of THz frequencies is the antenna size, which is reduced to sub-millimeters [12]. The implementation of these systems is now possible due to the advancements in the realization of the photonic and semiconductor devices with an operating frequency in the terahertz band [13]. A common approach is to design the antenna in a low loss substrate and then integrate it to the active devices. For contiuous-wave opetation, the ultrafast photoconductive material, such Low Temperature Grown (LTG)-Gallium Arsenide (GaAs), is situated at the driving point in THz antenna.

In order to understand the treatment of the antennas as circuit elements, differences between broadband and resonant antennas must be highlighted. In addition, it can be observed how this classification influences the treatment and analysis of certain antennas [14].

2.1 Resonance Antennas

A resonant antenna, or resonant-length antenna, is an antenna whose length is a quarter of a wavelength, or multiples thereof long. In this case, the antenna is purely resistive and its reactance is zero. As a result, the maximum amount of current flows through the antenna.

Higher R_A is directly reflected to better impedance matching which leads to maximizing the transmission of the THz output power through R_A [15]. Hence, over the different antenna geometries for antenna impedance maximisation, the full-wave dipole has been chosen for high impedance and easy modelling.

2.1.1 Full-Wave Dipole Antenna

A full-wave dipole in free space has a typical impedance of 710 Ω. However, using a dielectric substrate the impedance is reduced due to the increased effective permittivity. The antenna dimensions are listed in Table 2.1. Furthermore, the influence of the substrate thickness in the antenna features is shown in Table 2.2.

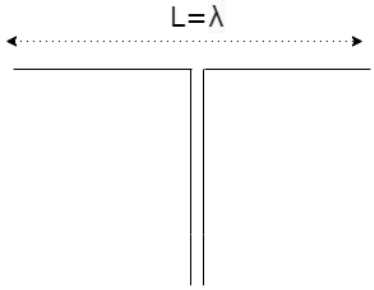

Figure 2.1: Full-wave dipole dimension

The chosen thickness of the substrate is 1 μm and the antenna impedance results 340 Ω. This membrane reduces the effect of permittivity and dielectric losses.

As the length of the dipole is based on the full-wave dipole, then $L = \lambda$. The dimensions of the structure of the Fig. 2.1 are shown in Table 2.1.

The design working on the cut-off of $f_0 = 1$ THz results:

$$\lambda_0 = \frac{c_0}{f_0} = 300\mu m \tag{2.1}$$

With the influence of the high permittivity LTG-GaAs substrate ($\varepsilon_r = 12{,}9$):

$$\lambda = \frac{\lambda_0}{\varepsilon_r} = 83.3\ \mu m \tag{2.2}$$

The antenna dimensions are listed in Table 2.1. Furthermore, the influence of the substrate LTG-GaAs thickness in the antenna features is shown in Table 2.2.

	Length	Width	Thickness
Dipole ($L = \lambda$)	83.3 μm	5μm	100 nm

Table 2.1: Dipole dimensions

Substrate Thickness (GaAs)	1 μm
Impedance	340 Ω
Gain	2.4 dBi
Bandwidth	29%

Table 2.2: Dipole features

The design has been implemented in $CST\ Studio$. As a result of the work, a low value of $S_{11} = -19{,}77$ dB working at resonance frequency (~ 1 THz).

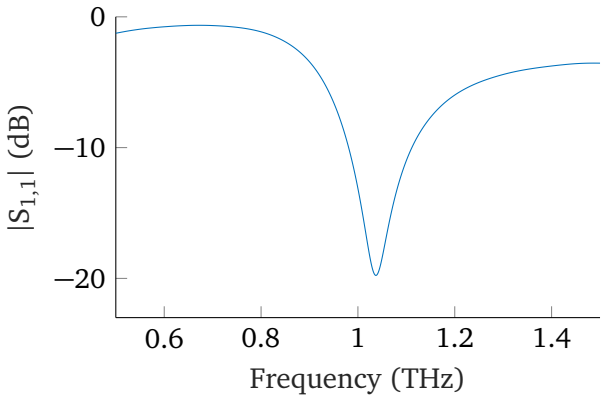

Figure 2.2: $|S_{1,1}|$ parameter of the Full-Wave dipole antenna

2.2 Broadband Antennas

One of the major points of interest in THz technology is the possibly of broadband spectroscopy by using the very wide tunability of LTG-GaAs based photomixers. However, this implies the use of frequency independent antennas to be able to exploit a broad frequency range.

Frequency independent antennas hold the radiation pattern as well as the impedance constant over frequency. The pattern problem is much more complex and more difficult than the impedance problem. A successful approach has been developed by [16] considering antenna shapes which depend on angles only.

It is more difficult to design broadband planar antenna with resistance larger than few hundred ohms. The impedance Z_{SC} of an antenna identical to its complement is independent of frequency and can be calculated:

$$Z_{SC} = \frac{1}{2}\sqrt{\frac{\mu}{\varepsilon}} \tag{2.3}$$

Therefore, any self-complementary antenna will have an impedance of 188.5 Ω in free space and 71.5Ω on a LTG-GaAs substrate with relative permittivity of $\varepsilon_r = 12.9$. All such antennas extend theoretical to infinity, as they are defined by angles only. This implicates one of the main problems on the frequency independent antennas: it is mandatory to determine the necessary physical length of an antenna which is a reasonable approximation of the infinite length. In effect, the current distribution remains constant with respect to wavelength over the finite geometry. Thus, the pattern and also the impedance of such antennas are practically independent of frequency above a certain value.

By the introduction of logarithmic repeated features into the antenna, the abrupt termination of all currents at its ends, which reduces the bandwidth by increasing the lowest usable frequency [17] is overcome. These teeth periodically positioned shorts out the current distribution along the antenna and corresponds to one quarter wavelength [17]. This distinguishes the antenna as one of the broad class of log-periodic antennas. However, the current density in the shorting teeth contributes to the total current distribution on the antenna and therefore also to the linear polarised radiation pattern.

2.2.1 Log-Periodic Circularly Toother Planar Antenna

The design of the log-periodic antenna is addressed to a broad frequency range with constant impedance and farfield pattern. In order to implement these properties the log-periodic antenna allows for varying design parameters, which is showed in Fig. 2.3. The lowest usable frequency is defined by the outermost tooth, which length has to be chosen to be one quarter-wavelength. The ration of edge distances τ is constant and defines the ration between the frequencies from two adjacent periods [17]:

$$\tau = \frac{R_{n+1}}{R_n} = \frac{f_n}{f_{n+1}} < 1 \tag{2.4}$$

And the slot width is expressed by:

$$\sigma = \frac{r_n}{R_n} < 1 \tag{2.5}$$

If α and β are chosen to satisfy $\alpha + \beta = 180$ the antenna is identical to its complement and becomes a self-complementary antenna, which tends to be frequency-independent [17].

For the realised design, the design parameters from Fig. 2.3 and the number of N teeth one side has been chosen to:

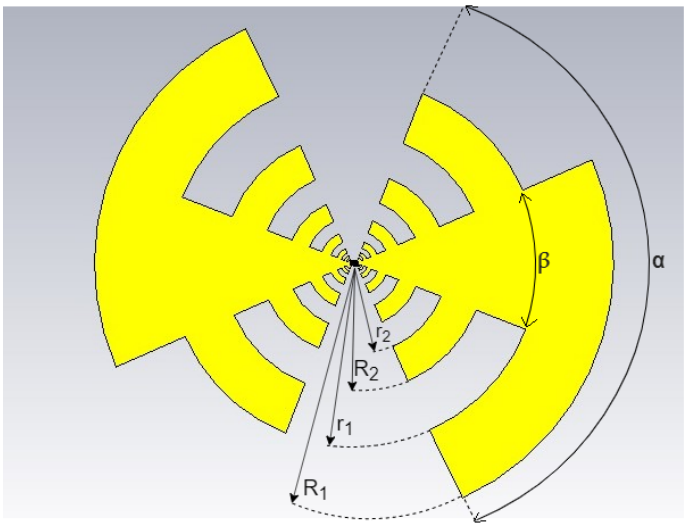

Figure 2.3: Log-periodic circular toothed planar antenna

α	150^o
β	50^o
τ	0.5
σ	$\sqrt{\tau} \approx 0.707$
R_1	640 μm
N	3

Table 2.3: Antenna parameters

These six parameters in Table 2.3 are sufficient for a complete description of the antenna geometry. Furthermore, the antenna has been implemented in $CST\ Studio$ as Fig. 2.4 shows.

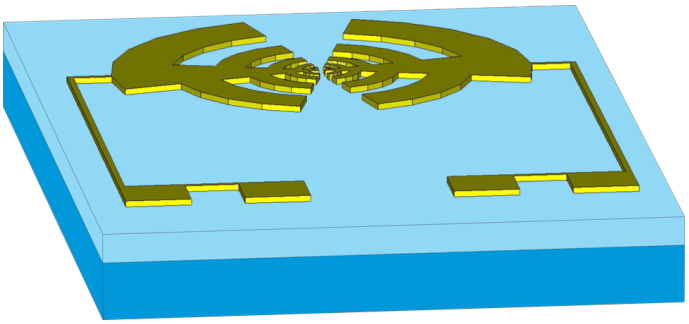

Figure 2.4: Log-periodic antenna on LTG-GaAs

3 THz Generation by Photomixing

Optical heterodyne conversion, or photomixing, is a frequency-agile technique that generates Continuous-Wave (CW) radiation at THz frequencies. Photomixers are compact, solid-state sources that use a pair of single-frequency, tunable lasers for THz different frequency generation by photoconductive mixing.

Features as spectral purity (e.g. linewidth), tuning range or bandwidth (i.e. the covered frequency range), output power over the efficiency, and even environmental or operation conditions (e.g. room temperature RT, cryogenic operation or high voltage) are adressed.

In GaAs the optical absorption is a fast process, whereas the electron-hole recombination lifetime is in the nanosecond range [18], which is one of the limitation factors.

The carrier lifetime should be in the sub-picosecond range, which is achievable by creating defects during *Molecular Beam Epitaxy* growth (MBE) LTG-GaAs [15]. Generally, LTG-GaAs samples have short carrier lifetime of $\sim$ 250 fs, high electric breakdown field of $> 5x10^5$ V/cm and high mobility of $200cm^2/V_s$ [19].

3.1 Work of Principle

Photoconductance in photomixing is modulated by optical beating of two laser sources with equal polarization that are heterodyned:

$$E_1(t) = E_0 e^{-i\omega_L t} \tag{3.1}$$

$$E_2(t) = E_0 e^{-i(\omega_L + \omega_{THz})t} \tag{3.2}$$

with $\omega_L = 2\pi f_L$ and $\omega_L + \omega_{THz} = 2\pi(f_L + f_{THz})$. When 3.1 and 3.2 are combined:

$$I_{tot}(t) = |E_1(t) + E_2(t)|^2 = 2E_0^2 \left| e^{-i\omega_L t}(1 + e^{-i\omega_{THz} t}) \right|^2 = 2E_0^2(1 + \cos[\omega_{THz} t]) \tag{3.3}$$

where $I_{L,0} = 2E_0^2$, finally is obtained:

$$I_{tot}(t) = I_{L,0}(1 + \cos[\omega_{THz} t]) \tag{3.4}$$

The semiconductor absorbs the laser signal and a DC bias is applied between photoconductor electrodes. Then, the modulation of the laser signal becomes AC current.

$$I_{Ph}(t) = \frac{eP_L(t)}{h\upsilon_L} = \frac{eP_{L,0}}{h\upsilon_L}(1 + \cos[\omega_{THz} t]) \tag{3.5}$$

Ideally, it would be $I_{AC} = I_{DC} = \frac{eP_{L,0}}{h\upsilon_L}$, and finally:

$$P_{THz}^{id} = \frac{1}{2} R_A I_{AC}^2 \tag{3.6}$$

3.2 THz Radiation

The radiation resistance of any arbitrary, non-magnetic material is given by $Z_M = \sqrt{\frac{\mu_0}{\varepsilon_r \varepsilon_0}} = \frac{377\Omega}{\sqrt{\varepsilon_r}} = \frac{377\Omega}{n}$, where 377 Ω is the air resistance Z_{air}.

The radiation is towards the substrate ($> 90\%$) because the substrate is better impedance-matched compared with the air. Now, reflection at backside is observed. This fact could be problematic because the exit of the THz-radiation has perpendicular incidence, with $R = \left(\frac{n-1}{n+1}\right)^2 = 31\%$ and angled incidence. In that case, small angles can derive into Fresnel laws, large angles cause total reflection and, finally, the critical angle coming from $\alpha_T = \arcsin(1/n) = 16{,}1^o$. Consequently, it causes ~ 2 orders of magnitude of loss

A solution to overcome this problem is by using a curved surface, such a lens (See 3.1). The refractive index of lens must be equal to the refractive index of the substrate. Usually highly resistive Silicon is used due to its poor absorbption. The main result is the loss of only $\sim 31\%$.

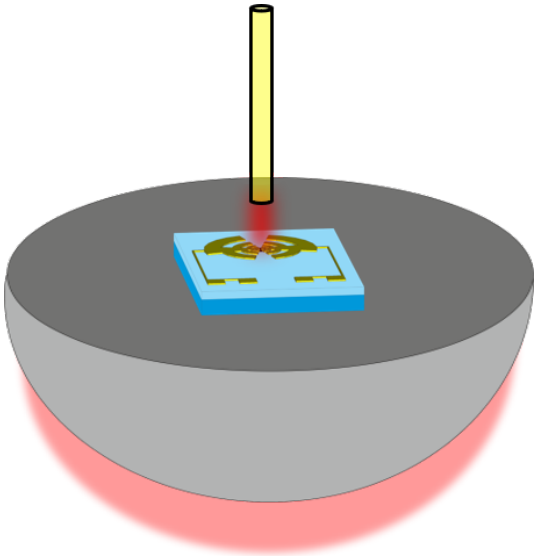

Figure 3.1: THz radiation antenna radiation with Si-Lens

Over the features of photomixer, can be highlighted the room temperature operation and the easy tunning of the lasers in the range of a few THz, e.g. $1550nm$ laser ($193THz$): $1THz$ – 0,5% easy. Also broadband antennas can be used with a huge bandwidths, with more that 2 orders of magnitude (e.g. $30GHz - 3THz$). The typical laser wavelengths used are $800nm$ (for Low Temperature Grown-GaAs) and $1550nm$ (InGaAs). The power levels are in the order of μW.

The most important requirement to be fulfulled is that the semiconductor device must be "fast" enough to be able to generate the THz AC current. Usually is not the case due to the trade-off with *RC-roll-off* and *transit-time* or *life-time roll-off*.

3.2.1 RC and Carrier Lifetime Roll-Off

Every semiconducting device has a certain capacitance. This capacitance is in parallel to antenna and typical values can be $C \sim 2{-}20fF$ and antenna with $R_A \sim 70\Omega$. The f_{RC}^{3dB} frequency, where the THz power is reduced by a factor of 2, is obtained with the formula $f_{RC}^{3dB} = \frac{1}{2\pi R_A C}$, with typical values of $110GHz \sim 1.1THz$.

So, the RC-roll-off is finally obtained with

$$\eta_{RC} = \frac{1}{1 + (2\pi f RC)^2} \tag{3.7}$$

As a result, at high frequencies $\eta_{RC} \sim f^{-2}$

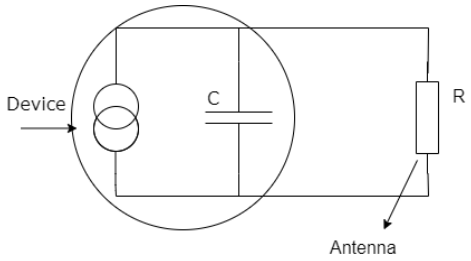

Figure 3.2: Equivalent circuit of the capacitance with the antenna

The origins of the capacitance are discussed in Section 3.3. On the other hand, there is the *transit-time* or *carrier lifetime*, which describes the "intrinsic speed" of the device.

$$\eta_{tr} = \frac{1}{1+(f/f_{tr}^{3dB})^2} \tag{3.8}$$

Typical values are $f_{tr}^{3dB} \sim 150GHz - 1THz$ and it can be derived at high frequencies that $\eta_{tr} \sim f^{-2}$.

Finally, the THz output power is

$$P_{THz}(\nu_{THz}) = \frac{1}{2} R I_{AC}^2 \eta_{RC} \eta_{tr} \tag{3.9}$$

3.3 Electrodes in THz Photoconductive Mixer

As explained before, light generates electron-holes pairs and an applied bias separates electrons from holes, generating the current. In other words, light switches the resistance of the semiconductor. Then, a field is required in order to separate electrons form holes and to generate the photocurrent. The typical size of the area is $10x10\mu m^2$, which corresponds to the size of the laser spot.

In contrast, a capacitance of electrode structure is generated comparing with the capacitance in the large area, which is negligible. Nevertheless, the main goal of the use of fingers are the **gain**, the **high frequency** and **lifetime roll-off**. In fact, fingerless structures are used for pulsed operation.

So, total current generated by the device is due because every moving carrier in the semiconductor induces a current at the electrodes. Indeed, currents from different places add up. However, it is showed a semiconductor with deep traps, whereas trapped carrier cannot move. There is no hopping between trap states and distances are too large. This fact does not contribute to current any more.

The time required to trap a carrier (on average) is called *lifetime* or *recombination time* (τ_{rec}). On the other hand, the time required to travel through the gap (on average) is called *transit time* (τ_{tr}). Conclusively, the goal is calculate current at the electrode because the $P_{THz} \sim I_{AC}^2$ [20]:

$$|I_{tot}| = \frac{\tau_{rec}}{\tau_{tr}} I_{id} \cos(\omega_{THz} t + \varphi) \frac{1}{\sqrt{1+(\omega_{THz}\tau_{rec})^2}} + \frac{\tau_{rec}}{\tau_{tr}} I_{id} \tag{3.10}$$

with $\varphi = \arctan(\omega_{THz}\tau_{rec})$. It is shown that AC and DC current reduced by $\frac{\tau_{rec}}{\tau_{tr}} \equiv g \longrightarrow$ "photoconductive gain". Typical values are $g \sim 10^{-2} - 10^{-3}$. Thus, THz power rolls off as:

$$\eta_{LT} = \frac{1}{1+(2\pi\tau_{rec}f)^2} \tag{3.11}$$

Low lifetime does not make sense at all, but when checking frequency behaviour:

$$P_{THz} = \frac{1}{2} R_A I_{id}^2 \left(\frac{\tau_{rec}}{\tau_{tr}} \right)^2 \eta_{LT} \tag{3.12}$$

$$f >> \Longrightarrow P_{THz} \simeq \frac{1}{2} R_A I_{id}^2 \left(\frac{1}{2\pi \tau_{tr} f} \right)^2 \neq f(\tau_{rec}) \tag{3.13}$$

$$f << \Longrightarrow P_{THz} \simeq \frac{1}{2} R_A I_{id}^2 \left(\frac{\tau_{rec}}{\tau_{tr}} \right)^2 \sim \tau_{rec}^2 << \tag{3.14}$$

Short lifetime seems to be no help at high frequencies and does even reduce P_{THz} at low temperatures. However, heat deposition in samples is neglected so far. As it is shown in:

$$I_{DC} = g I_{id} << I_{id}$$

The heat deposited is given by:

$$P_H = I_{DC} U_{DC} + P_L$$

where U_{DC} is the bias applied to electodes and P_L is the optical power.

A strong reduction of electrical heat by low life-time is achieved as $P_{EI} = g I_{id} U_{DC} << I_{id} U_{DC}$. For instance, much higher DC bias can be tolerated and much higher optical power can be used. Consequently, much mure THz power is generated.

Hence, in order to see which structure is better to use for CW, it is needed to take into account that small gap increases gain without affecting carrier lifetime (τ_{tr} – ω_g and g - $1/\omega_g$). Therefore, small gaps are preferred, but not too small because of the capacitance and area of the optical spot needs to be covered, explaining the use of the fingers.

Different types of CW THz photomixers LTG-GaAs based are implemented Chapter 4. First, using metal interdigitated electrodes and second, with single nanowire (Ø 120nm). The small diameter of the nanowire reduces the device capacitance by a factor of more than 10 compared to photomixers with conventional interdigital fingers, which offers high reliable operation.

4 Photomixer Integration and Antenna Matching

Photoconductive antennas are one of the most promising and typically used means for the generation of terahertz. This fact is due to its high performance capability and compact optical sources with pulse operation and continuous waves that are needed for broadband and narrowband terahertz generation [21].

One of the most relevant challenges in the design of photoconductive antennas at THz applications is the trade-off between the parasitic capacitances with the introduction of photomixers and the THz output power. As explain in Chapter 3, the narrow gaps between the electrodes are used in order to obtain a short transit time. Thus, the photoconductive gain is increased at a fixed photocarrier lifetime. However, this fact introduces an internal capacitance, which plays an important part in the photomixer operation. Indeed, its parasitic capacitance response acts as a short circuit to the antenna impedance [15].
Hence, if the value capacitance of the device is high, the value of the THz output power would be affected. That is why new optimized designs of photomixer are required in order to decrease the capacitance and maintain the high photoconductive gain [22].

The design and integration of a planar logarithmic-periodic circular toothed antenna (PLPCTA) with plasmonic contact electrodes has the purpose of keep high radiation power levels over a wide frequency range. The antenna has a broadband radiation resistance of 70–100 Ω and a relatively low reactance level over the 0.1–2 THz range [23].

However, comparing with the antenna, the photomixer has a larger impedance caused by its specific structure. Consequently, the real part of the impedance and the influence of the parasitic capacitance of the photomixer are taken into account, as it is shown in Fig.4.1.

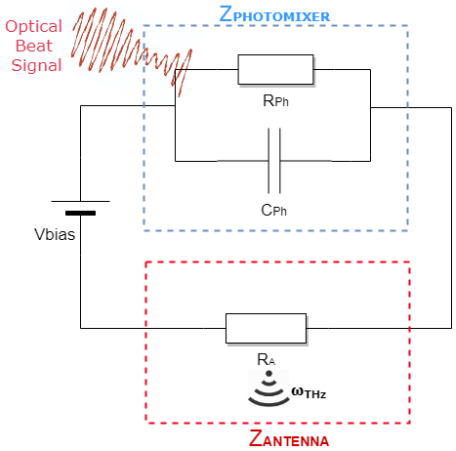

Figure 4.1: Schematic circuit of the photomixer and the radiating antenna.

In 2.2.1, it has been shown that the impedance of the planar logarithmic-periodic circular toothed antenna at free space, using the equation 4.1 has value of 188.5Ω [24].

$$Z_{SC} = \frac{1}{2}\sqrt{\frac{\mu}{\varepsilon}} \tag{4.1}$$

However, as the antenna is LTG-GaAs based, with a relative permitivity ε_r of 12.9, the real part of the antenna impedance finally has a value of 71,5Ω.

Impedance matching is an afterthought at lower and medium frequencies. However, impedance matching is a challenge of RF and microwave circuit design because the error threshold decreases as frequency increases. For instance, as it is mentioned before, the photomixer impedance is larger than the antenna and the discontinuities in the physical path of transmission, due to the difference of dimensions, are presented between both elements. This leads to high mismatching and, consequently high power losses [25]. In other words, it is necessary to match the impedance of the load (radiating antenna) to the source (photomixer) in order to maximize the power transference, which becomes immensely critical in ultra-high frequency designs.

The determination of the equivalent impedance of the photomixer $Z_{Ph} = R_S + jX_S$ is done by calculating the parallel of its capacitance C_{Ph} and intrinsic resitance R_{Ph}, shown in Fig.4.2.

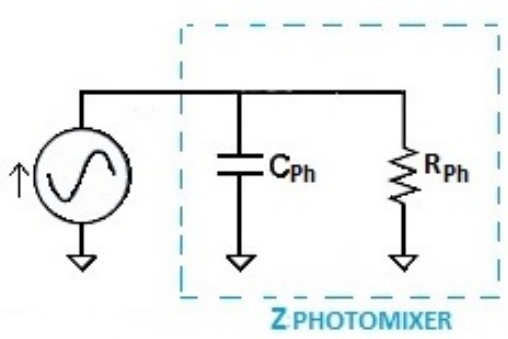

Figure 4.2: Equivalent impedance of the photomixer.

There are many different techniques for impedance matching, and the best application of each will depend on the situation. Indeed, the solution of this problem in this case is the design of a Highpass matching network shown in Fig.4.3, using lumped elements as inductors and capacitances. The use of an online tool for the design (see [26]) with an input values of the equivalent impedance of the photomixer $Z_{Ph} = R_S + jX_S$ and the antenna resistance $R_{Antenna} = R_L$, together with the Q desired and a working frequency of 1 THz, different values of C and L are obtained.

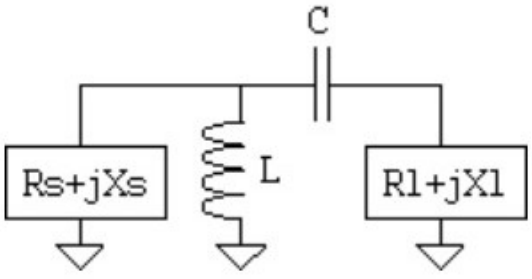

Figure 4.3: Highpass matching network.

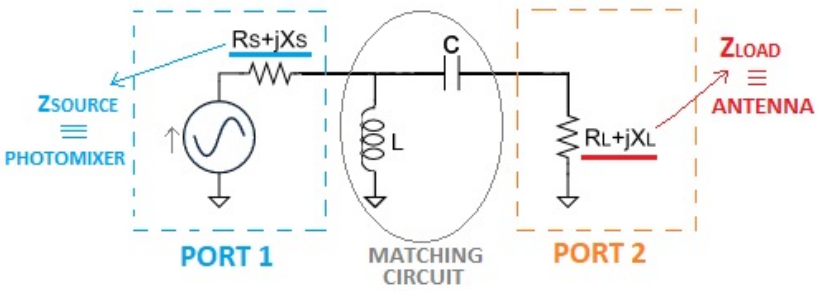

Figure 4.4: Equivalent Matching Circuit.

For the simulation of the matching circuit designed, a Microwave Office Software has been used. *National Instruments AWR Design Environment*^{TM} Software is focused on radio frequency (RF), microwave and high frequency analog circuit and system design. The generic schematic matching circuit for the different designs is shown in Fig. 4.5.

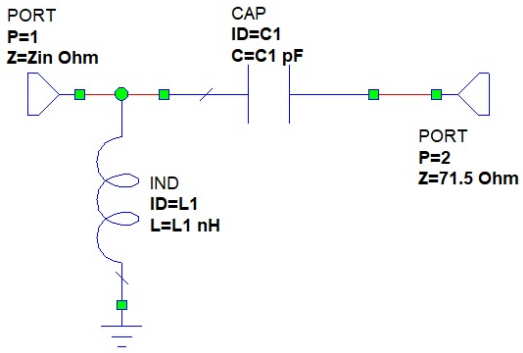

Figure 4.5: NI AWR schematic circuit.

4.1 Finger-electrode Photomixer

For an undoped and infinitely thick semiconductor, the capacitance of the quasi-static interdigital-finger electrode [15] can be calculated using a simplified conformal mapping technique [27] as

$$C \simeq \frac{\pi\varepsilon_0(1+\varepsilon_r)A}{2(w_e+w_g)\log\left(\frac{2(1+\sqrt{k})}{1-\sqrt{k}}\right)} \tag{4.2}$$

where w_e and w_g are the finger electrode and gap width, respectively. ε_0 is the absolute permittivity and ε_r is the relative permittivity of LTG-GaAs with a value of 12.9. A is the active area of the photomixer, calculated as $A = [N_e w_e + (N_e - 1)w_g]^2$. When $w_e < w_g$, k can be calculated as

$$k = \sqrt{1 - \tan^4\left(\frac{\pi w_e}{4(w_e+w_g)}\right)} \tag{4.3}$$

The capacitance according with the finger and gap dimensions (see Fig. 4.6) is finally obtained for both designs, with a value of $C \approx 2.95$ fF.

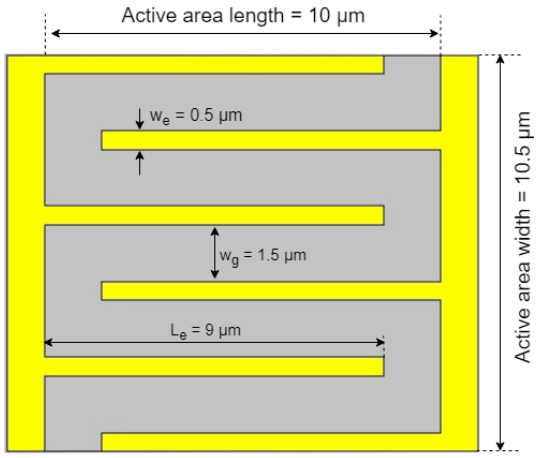

Figure 4.6: Interdigital electrode photomixer dimensions

The Scattering parameters or S-parameters (the elements of a dispersion matrix or S-matrix) describe the electrical behaviour of linear electricity networks when are subjected to several steady state stimuli by electrical signals. The parameters are useful for various branches of electrical engineering, including electronics,

communication system design, and in particular for microwave engineering. In other words, S-parameters basically describe the I/O relationship between ports (or terminals) of an electrical system [28].

In this context, a port can be defined as any place where voltage and current can be delivered. For example, if there are 2 ports in a network, (called Port 1 and Port 2), then S_{12} represents the power transferred from Port 2 to Port 1. S_{11}, therefore, is the reflected power that Port 1 is trying to deliver to Port 1. On the other hand, S_{21} would represent the power transferred from Port 1 to Port 2. In general, S_{NM} expresses the power transferred from Port M to Port N in a multiport network. Hence, note that, in general, S-parameters are a frequency dependent (i.e. they vary with frequency).

In practice, S_{11} is the most commonly used parameter in the antenna environment. Generally, indicates the power reflected from the antenna after the transmission occurs. It is also known as the reflection coefficient.

Since antennas are generally designed to be low-loss, so ideally most of the power delivered to the antenna should be radiated. See also $VSWR$, which is directly related to S_{11}. Therefore, in order to analyze the above mentioned adaptive networks, the S parameters have been simulated with the help of NI AWR software. The input values are shown in Table 4.1.

R_{Ph}	10kΩ
C_{Ph}	3 fF
Z_{in}	$0.281 - j53.05\ \Omega$
L_1	0.00793 nH
C_1	0.000188 pF

Table 4.1: Values of lumped elements of interdigitated photomixer.

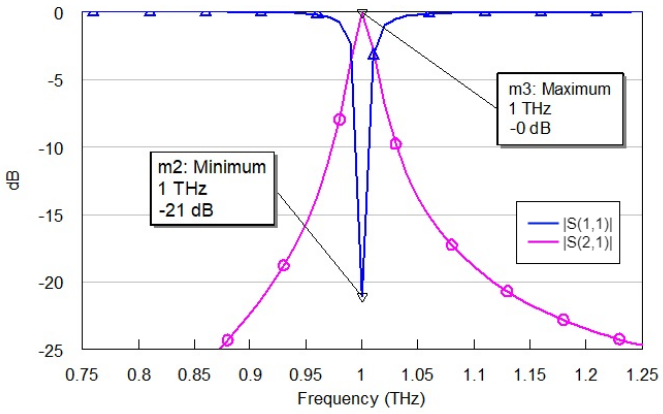

Figure 4.7: Impedance matching circuit between antenna with interdigital photomixer

The Fig. 4.7 implies that the antenna radiates best at 1 THz, where $S_{11} = -21$ dB. Furthermore, at 800 GHz the antenna will radiate virtually nothing for both cases, as S_{11} is close to 0 dB (so all the power is reflected). The antenna bandwidth can also be determined from the Fig. 4.7. If the bandwidth is defined as the frequency range where S_{11} is to be less than -10 dB, then the bandwidth would be roughly 20 GHz. Regarding the S_{21}, as is equal 0 dB, implies that all the power delivered to port 2 (antenna) ends at the terminals of port 1.

4.1.1 Plasmonic effect

The plasmonic effect is known [29] as the interaction between the free resonant oscillation of conduction electrons of a metal, excited by the interactive electromagnetic field at a metal/dielectric interface, and incident light. The phenomenom of Surface Plasmon Resonance (SPR) is derived from this effect [30].

The first implementation inside the gap of THz antenna are interdigitated electrodes, or as they often called, "fingers". Such structures, especially metal, when exposed to an external electromagnetic field provide strong field localization in the gap between the nanoparticles. As result, a large value of the absorption cross section of quantum detector placed in the gap, based on the plasmonic effect. Due to this property, they are used in THz photoconductive antennas and photomixers, enhancing an optical field of pump laser and redistributing it into the surface layer of the semiconductor substrate near the electrodes [31].

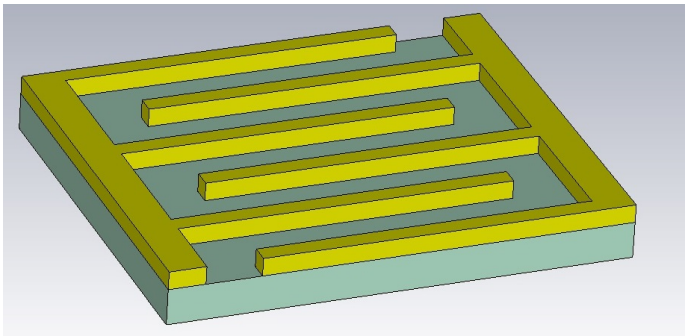

Figure 4.8: 6 finger Au structure.

The rapid increase in the charge carriers concentration leads to a huge impulse of the photocurrent that is much greater than in conventional THz antennas. The amplitude of THz field is directly proportional to the rate of change of the photocurrent density, according to :

$$E_{THz} \sim \frac{d(q_{e,p}, v_{e,p}, n_{e,p})}{dt}$$

where E_{THz} is the amplitude of the output THz signal, t is the process duration, resulting an increase of the efficiency of optical-to-terahertz conversion. It is important to note that physical dimensions of the nanoantennas and the material they are made of play an important role in the excitation of plasmon resonance. It is shown in Fig. 4.9 behaviour of the structure.

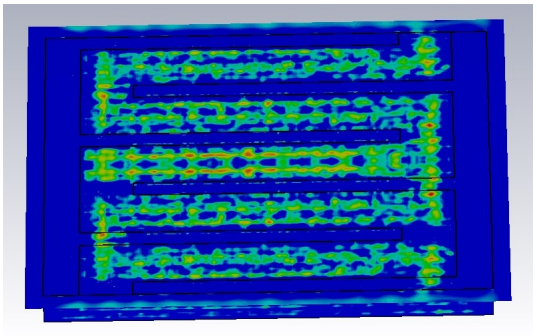

(a) top view

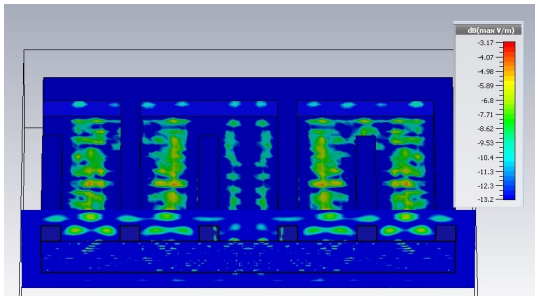

(b) cross section

Figure 4.9: CST simulation of the 6-finger photomixer

4.2 Ag-Nanowire Photomixer

As explained before, the capacitance of the photomixer shows up as a shunt capacitance that acts as a short-circuit at high frequencies. As a consequence, the output power of the device is affected. The nanowire photomixer has a much lower capacitance compared to the previously calculated interdigital photomixers. This is due to the reduction of the electrode dimensions by a minimum of one order of magnitude. Thus, among the most significant advantages of nanowire electrodes over interdigital electrodes, can be highlighted the small capacitance of the device with < 0.1 fF and the high photocurrent > 5 mA.

A new photomixer structure composed of a single nanowire on LTG-GaAs with a nanowire diameter of 120 nm and an electrode spacing of 1 μm has been designed. An alternative and simpler configuration was realised using a single Ag-NW with a diameter of 120 nm connected to one of the DC contacts. The gap to the second DC contact (tip-contact) was 2 μm. (see Fig. 4.10) The small diameter of the nanowire reduces the capacitance of the device by a factor of more than 10 compared to conventional interdigital finger photomixers [32].

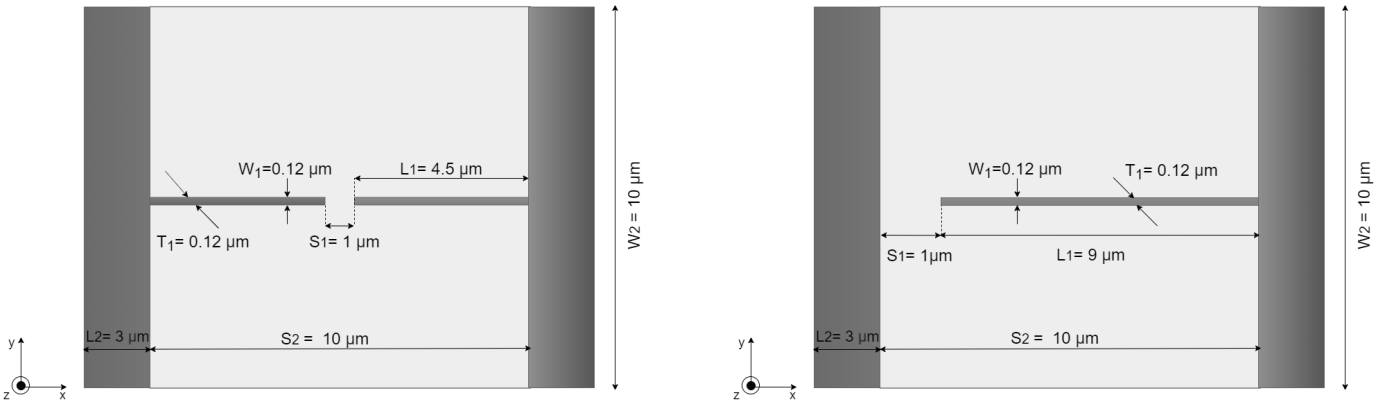

Figure 4.10: Tip-tip and Tip-contact Ag-NW photomixer, respectively.

The nanowire based photomixer capacitance is the summation of two parallel capacitances, one comes from the NW electrodes (C_1) and the other from the DC bias contacts (C_2) [33]:

$$C_T = C_1 + C_2$$

In order to do a better estimation of the capacitance value, a field-based capacitance model [34] was used for the structure of Fig.4.10. The total capacitance is given by:

$$C_i = \varepsilon_0 \varepsilon_r T_i \left(\frac{W_i}{S_i} + \frac{2}{\pi} \ln(1 + \frac{2L_i}{S_i}) \right) + \frac{3}{\pi} + \frac{1}{\pi} \ln \left(1 + \frac{\pi W_i}{2(1+\pi)(\frac{S_i}{2} + L_i)} \right) \tag{4.4}$$

where i is an interation number (1 or 2), ε_0 is the absolute permittivity, ε_r is the relative permittivity of the substrate, T_i is the physical electrode thickness, L_i is the physical electrode length, S_i is the gap between the electrodes, W_i is the physical electrode width.

As the first approximation, the field-based capacitance model (Eq. 4.4) ($i = 1$) is used to estimate the NW electrode capacitance value to $C_1 = 0.036$ fF, where $T_1 = W_1 = 0.12$ μm, $S_1 = 1$ μm, $L_1 = 4.5$ μm and $\varepsilon_r = 13$ for LTG-GaAs. The same approach ($i = 2$) was used to calculate $C_2 = 0.034$ fF< where $W_2 = 10$ μm, metallization thickness $T_2 = 0.12$ μm, $S_2 = 10$ μm, and $L_2 = 3$ μm as shown in Fig.4.10 (left). The sum of these both capacitances was 0.07 fF.

The field-based capacitance model in Eq. 4.4 used the fact that the width W is much larger than the gap S, which is not valid for the NW-based photomixer where $W \leq S$. A second fringe capacitance around the

gap (in the y–z axis) has to be added, which is similar to the first calculated value. The resulting total capacitance is $C_T = 0.14$ fF.

Same procedures were applied to the photomixer configuration tip-contact, shown in Fig. 4.10 (right). This configuration produces also two parallel capacitances, one between the NW gap and DC contact and the second capacitance between the two DC contacts. The Equation 4.5 is used to calculate C_1 for the tip-contact configuration.

$$C_i = \varepsilon_0 \varepsilon_r T_i \left(\frac{W_i}{S_i} + \frac{4}{\pi} \ln(1 + \frac{L_i}{S_i}) \right) + \frac{4}{\pi} + \frac{4}{\pi} \ln\left(1 + \frac{\pi W_i}{2(1+\pi)(S_i + L_i)}\right) \tag{4.5}$$

However, C_2 has the same value like in tip-tip configuration of $C_2 = 0.034$ fF. The total capacitance value obtained is $C_T = 0.21$ fF.

Once all capacitances are theoretically calculated, the designed and discussed adaptive network at the begining of the Section 4 has been performanced. The used values are shown in Table 4.2. The S-parameters have been simulated with the help of *NI AWR* software, shown in 4.11.

	Tip-Tip Ag-NW	Tip-Contact Ag-NW
R_{Ph}	4kΩ	4kΩ
C_{Ph}	0.14 fF	0.21 fF
Z_{in}	$298.944 - j1051.859\Omega$	$152.2870 - j765.4781\Omega$
L_1	0.0511 nH	0.05819 nH
C_1	0.0003 pF	0.0003 pF

Table 4.2: Values of lumped elements of Ag-Nanowire photomixers.

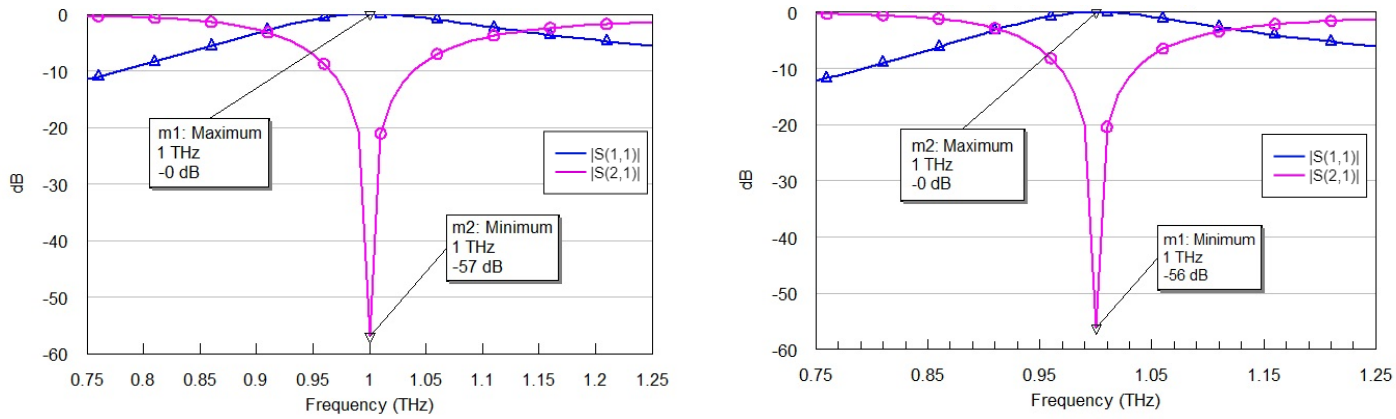

Figure 4.11: Impedance matching circuit between antenna with Tip-Tip and Tip-Contact Ag-NW photomixer, respectively

The results show that the antenna radiates best at 1 THz, where $S_{11} = -57$ dB in the case of tip-tip Ag-NW, and $S_{11} = -57$ dB for tip-contact Ag-NW photomixer. Furthermore, at 800 GHz the antenna will radiate virtually nothing for both cases, as S_{11} is close to 0 dB (so all the power is reflected). The antenna bandwidth can also be determined from the Fig. 4.11. If the bandwidth is defined as the frequency range where S_{11} is to be less than −10 dB, then the bandwidth would be roughly 70 GHz for both cases. Respect to the S_{21}, as is equal 0 dB, implies that all the power delivered to port 2 (antenna) ends at the terminals of port 1.

4.2.1 Plasmonic effect

Plasmonic metal nanostructures such as nanoparticles (NPs), nanorods (NRs), and nanowires (NWs) have been introduced in order to improve device efficiency via nanoscale light confinement [35].

Among various metal nanostructures, silver nanowires (AgNWs) are considered promising plasmonic materials with strong surface plasmon resonance (SPR) spanning the visible spectrum and near-infrared region [36].

The main advantage of AgNW networks is that is considered as an excellent transparent electrode as well as a plasmonic nanostructure for high-performance optoelectronic devices [37].

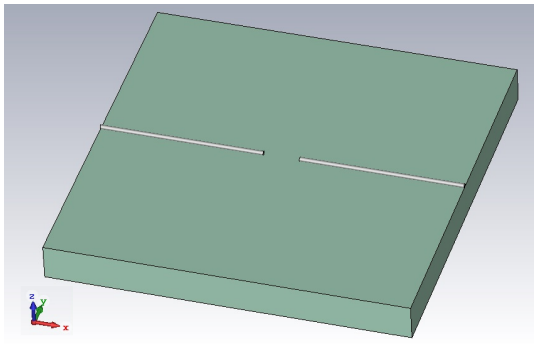

(a) Tip-tip Ag-Nanowire.

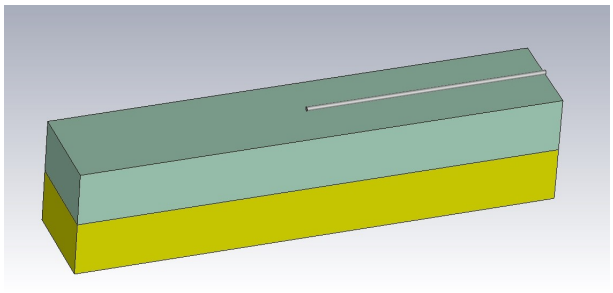

(b) Tip-contact Ag-Nanowire with Au-backside metalisation.

Figure 4.12: 3D CST design of the Ag-NW photomixers

This structure is able to resonantly enhance scattered light and local electromagnetic fields (E-field) and provide large E-field enhancements [38, 39]. In particular, can act as efficient nanoantenna to couple the incident light into propagating surface plasmon polaritons (SPPs) on metal NWs surfaces [40]. This fact can improve resonant coupling to excitons in the organic semiconducting active layer, resulting in increased photogeneration of charge carriers or increased radiative emission [41].

For the design of the structure, it has been used a substate of LTG-GaAs ($\varepsilon_r = 12.9$), with a thickness of 1 μm and diameter of the Ag-NW of 120 nm, as it is shown in Fig. 4.12a. On the other hand, in Fig 4.12b, the substrate has a thickness of 1 μm, with a backside metalisation of gold also of 1 μm. The simulations can be found on Fig. 4.13 and Fig 4.14, repectively.

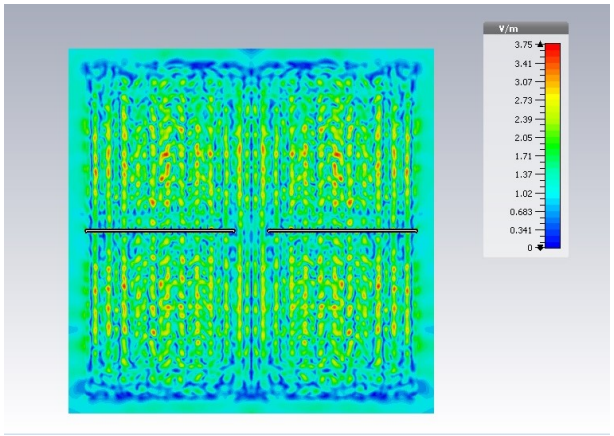

(a) top view

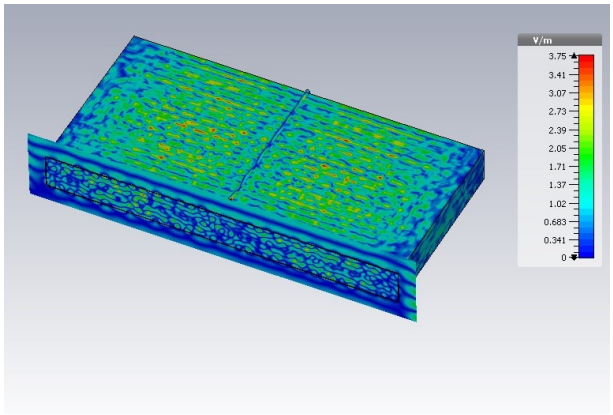

(b) cross section

Figure 4.13: CST simulation of the tip-tip Ag-Nanowire photomixer.

To summarize the plasmonic results, it can be affirmed that:

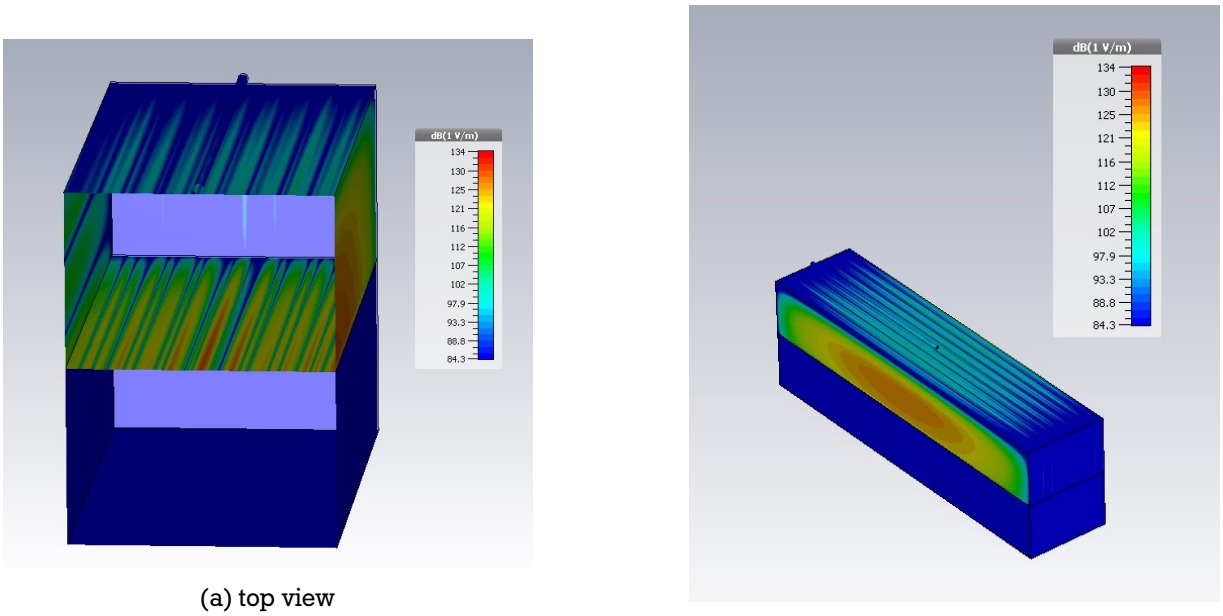

(a) top view

(b) cross section

Figure 4.14: CST simulation of the tip-contact Ag-Nanowire photomixer with Au-metallisation.

- Plasmonic metallic nanostructures have attracted considerable attention in photovoltaic areas due to their strong interactions with light through excitation of surface plasmon resonance (SPR) [30].
- The frequency and intensity of SPR are strongly related to the size, composition, shape, and the nature of metallic nanostructures, making it possible to design plasmonic structures that interact with the entire solar spectrum and beyond.
- Due to their intriguing photoactive properties, plasmonic metal nanostructures have been assembled with semiconductors to construct materials for visible-light-responsive electrodes.
- SPR induces light absorption and subsequent transfer of hot electrons from the plasmonic nanostructures to the conduction band of the semiconductors in contact.
- Near-field electromagnetic enhancement can amplify the absorption of light and increase the generation and separation rates of electron–hole pairs in the semiconductor.
- Because the SPR intensity is not strong enough to harvest sufficient incident light, it is about to optimize the SPR intensity and range of the plasmonic nanostructure, the design of the photoelectrode structure for enhancing the SPR effects and increasing the efficiency energy use by plasmonic metallic nanostructures.

4.3 Antenna Matching

As it has been achieved the theoretical design of the antenna matching, now the practical implementation is going to be shown in this chapter. Over the multiples techniques that exist to create a real matching circuit, it is required to be taking into account the dimensions of the working antenna.

The antenna size is ~ 10 times larger than the photomixer. This fact is quite important, as it highly restricts the techniques that are allowed to be used for matching.

In the first instance, there is the **stub** or **resonant stub**, which is used to implement those circuits.

It consist of a length of transmission line or waveguide that is connected at one end only [42]. The free end of the stub is either left open-circuit or (always in the case of waveguides) short-circuited.

In case of neglecting the losses of the transmission line, the input impedance of the stub is purely reactive; either capacitive or inductive, depending on the electrical length of the stub, and on whether it is open or short circuit. Stubs can either work as capacitors, inductors and resonant circuits at radio frequencies.

Often are used to replace dicrete capacitors and inductors because UHF and microwave frequencies lumped components perform poorly due to the parasitic capacitance.

Therefore, and explained before, they are used mainly in antenna impedance matching circuit, but also are common in frequency selective filters, resonant circuits for UHF electrons oscillators, and radiofrequency amplifiers.

4.3.1 Stubs

The behavior of short and open stubs, as stated before, is explained by means of transmission lines theory. The mathematical development of the following equation can be found in any book dealing with fundamentals in microwave engineering. Mainly, in a lossless transmission line it is possible to propagate the impedance between two points z_1, z_2 along the line, which are separated by a distance $l = z_1 - z_2$, using the following formula:

$$Z_1 = Z_2 \frac{Z_0 + jZ_0 \tan\beta l}{Z_0 + jZ_2 \tan\beta l} \tag{4.6}$$

For stub-based impedance matching, Z_2 is open or short, thus being able to tune the resulting impedance at the entrance of the stub, Z_1, to the desired inductive value.

Open circuited stub

An open circuit has an infinite impedance, $Z_{\text{open}} = \infty$. Thus, in equation 4.6 Z_2 has this value, which results in an indetermination of type ∞/∞. After applying L'Hopital, the input impedance of a lossless short circuited line results in:

$$Z_{OC} = -jZ_0 \cot(\beta l) \tag{4.7}$$

The length of a stub to act as an inductor L at the same frequency is thus given by:

$$l = \frac{1}{\beta}\left((n+1)\pi - \operatorname{arccot}\left(\frac{\omega L}{Z_0}\right)\right) \tag{4.8}$$

where β is the propagation constant $\beta = \frac{2\pi f}{\lambda}$ working with a resonance frequency of 1 THz, Z_0 refers to the characteristic impedance of the antenna log-periodic, which is discussed in Chapter 4, has a value of 70,1 Ω. L is obtained from the Table 4.1, with an average value of 8 pH. The length of the open circuited stub obtained is finally 148 μm.

Short circuited stub

For a shorted circuit, the impedance is $Z_{\text{short}} = 0$. Therefore, after substituting Z_2 by this value, equation 4.6 reduces to:

$$Z_{SC} = jZ_0 \tan(\beta l) \tag{4.9}$$

The length of an open circuit stub to act as an inductor L at an angular frequency of ω is:

$$l = \frac{1}{\beta}\left(n\pi + \arctan\left(\frac{\omega L}{Z_0}\right)\right) \tag{4.10}$$

where $\beta = \frac{2\pi f}{\lambda}$, $f = 1THz$, $Z_0 = 70{,}1\Omega$ and L is also obtained from the Table 4.1, with an average value of 8 pH. The length of the short circuited stub obtained is finally 188 μm.

Observing the results, it can be appreciated that the measurements obtained are close to the physical size of the antenna. This fact makes the implementation of the adaptation non-viable, since there is not enough physical space between the antenna and photomixer.

In light of the above, the needed matching network to achieve a good power transfer between the antenna and photomixer is not implementable using stubs. One possible solution would be to implement the stubs in microstrip technology, using a substrate with very high dielectric permittivity ε_{r}, which decreases the needed stub length. This can be seen when substituting $1/\beta$ in equations 4.8 and 4.10:

$$l = \frac{1}{\beta}[\ldots] = \frac{\lambda}{2\pi f}[\ldots] = \frac{1}{\sqrt{\varepsilon_{\text{r}}}}\frac{\lambda_0}{2\pi f}[\ldots] \tag{4.11}$$

However, further design by using high-ε_r materials lies outside of the focus of this document and thus it is not further addressed.

5 Conclusion and Outlook

This work describes CW emitters that work according to the principle of photomixing. The photoconductor, electrode geometry and antenna have each been independently optimized according to the individual criteria from the theoretical model. There are advantages in using CW-THz radiation for commercial imaging and spectroscopy systems, compared to the more established pulsed technologies.

THz technology focuses its interest in the possibility of broadband spectroscopy by using the very wide tunability of LTG-GaAs based photomixers. Frequency independent antennas hold the radiation pattern as well as the impedance constant over frequency. The design of the log-periodic antenna is addressed to a broad frequency range with constant impedance and farfield pattern. The possibilities of implementing a lumped element matching network are discussed. The values obtained of the matching elements are, for the interdigital photomixer $L = 7.93$ pH and $C = 1.88$ fF, and for the single nanowire $L = 50$ pH and $C = 0.3$ fF. Moreover, the low power transfer between the photomixer and antenna has been described, focusing in why classical distributed matching networks based in transmission lines are not suitable for this application, since they are simply too large to be used.

Ag-NW represents a promising nano-material for new plasmonic devices. The advantages of nanophotomixer instead of a classical metal electrode photomixer can improve the THz output power by reliable operation conditions at high optical power and high photocurrent. Plasmonic contact nanoelectrodes can enhance quantum efficiency and ultrafast operation compared to conventional photomixers. An example of this field is presented in this work in connection with THz-generation by optical mixing. The Ag-NW electrode with a physical diameter of 120 nm provides a device capacitance of 0.1 fF, which is more than ten times lower compared with interdigital six-finger electrodes.

The field of plasmonic requires now many new concepts in engineering applications in order to exploit many opportunities of optics and THz frequencies. New antenna designs and nanoelectrode photomixers with Ag-NW can be optimized by new matching elements for better THz power transfer and radiation.

This work can go further in some research directions in THz implementation of antenna and photomixers using nanoelectrodes. The suggested future work goes from new nanoelectrode configuration to new antenna design, where the extension of the operation frequency is expected.

Bibliography

[1] P. U. Jepsen, D. G. Cooke, and M. Koch, "Terahertz spectroscopy and imaging–modern techniques and applications," *Laser & Photonics Reviews*, vol. 5, no. 1, pp. 124–166, 2011.

[2] C. A. Schmuttenmaer, "Exploring dynamics in the far-infrared with terahertz spectroscopy," *Chemical reviews*, vol. 104, no. 4, pp. 1759–1780, 2004.

[3] P. H. Siegel, "Terahertz technology," *IEEE Transactions on microwave theory and techniques*, vol. 50, no. 3, pp. 910–928, 2002.

[4] M. Van Exter, C. Fattinger, and D. Grischkowsky, "Terahertz time-domain spectroscopy of water vapor," *Optics letters*, vol. 14, no. 20, pp. 1128–1130, 1989.

[5] B. Ferguson and X.-C. Zhang, "Materials for terahertz science and technology," *Nature materials*, vol. 1, no. 1, p. 26, 2002.

[6] K. Coppin, J. Geach, I. Smail, L. Dunne, A. Edge, R. Ivison, S. Maddox, R. Auld, M. Baes, S. Buttiglione *et al.*, "Herschel-astrophysical terahertz large area survey: detection of a far-infrared population around galaxy clusters," *Monthly Notices of the Royal Astronomical Society*, vol. 416, no. 1, pp. 680–688, 2011.

[7] U. U. Graf, C. E. Honingh, K. Jacobs, and J. Stutzki, "Terahertz heterodyne array receivers for astronomy," *Journal of Infrared, Millimeter, and Terahertz Waves*, vol. 36, no. 10, pp. 896–921, 2015.

[8] A. Smirnov, A. Baryshev, S. Pilipenko, N. Myshonkova, V. Bulanov, M. Arkhipov, I. Vinogradov, S. Likhachev, and N. Kardashev, "Space mission millimetron for terahertz astronomy," in *Space Telescopes and Instrumentation 2012: Optical, Infrared, and Millimeter Wave*, vol. 8442. International Society for Optics and Photonics, 2012, p. 84424C.

[9] J. Federici and L. Moeller, "Review of terahertz and subterahertz wireless communications," *Journal of Applied Physics*, vol. 107, no. 11, p. 6, 2010.

[10] S. Koenig, D. Lopez-Diaz, J. Antes, F. Boes, R. Henneberger, A. Leuther, A. Tessmann, R. Schmogrow, D. Hillerkuss, R. Palmer *et al.*, "Wireless sub-thz communication system with high data rate," *Nature photonics*, vol. 7, no. 12, p. 977, 2013.

[11] C. W. Berry and M. Jarrahi, "Terahertz generation using plasmonic photoconductive gratings," *New Journal of Physics*, vol. 14, no. 10, p. 105029, 2012.

[12] C. A. Balanis, *Antenna Theory: Analysis and Design*. Wiley Publishers, Hoboken, NJ, USA, 2017.

[13] H. Vettikalladi, W. T. Sethi, A. F. B. Abas, W. Ko, M. A. Alkanhal, and M. Himdi, "Sub-thz antenna for high-speed wireless communication systems," *International Journal of Antennas and Propagation*, vol. 2019, 2019.

[14] T. J. Rouphael, "Chapter 1 - antenna systems, transmission lines, and matching networks," in *Wireless Receiver Architectures and Design*, T. J. Rouphael, Ed. Boston: Academic Press, 2014, pp. 1 – 60. [Online]. Available: http://www.sciencedirect.com/science/article/pii/B9780123786401000019

[15] S. Al-Daffaie, "Nanoelectrode based photomixer for continuous wave terahertz generation," Ph.D. dissertation, TU Darmstadt, Göttingen, 2015, zugl.: Darmstadt, Technische Universität, Diss. 2015. [Online]. Available: http://tubiblio.ulb.tu-darmstadt.de/76169/

[16] V. Rumsey, "Frequency independent antennas," in *1958 IRE International Convention Record*, vol. 5. IEEE, 1966, pp. 114–118.

[17] R. Duhamel and D. E. Isbell, "Broadband logarithmically periodic antenna structures," 1957.

[18] J. Blakemore, "Semiconducting and other major properties of gallium arsenide," *Journal of Applied Physics*, vol. 53, no. 10, pp. R123–R181, 1982.

[19] S. Verghese, K. A. McIntosh, and E. R. Brown, "Optical and terahertz power limits in the low-temperature-grown gaas photomixers," *Applied Physics Letters*, vol. 71, no. 19, pp. 2743–2745, 1997. [Online]. Available: https://doi.org/10.1063/1.120445

[20] S. Preu, G. H. Döhler, S. Malzer, L. J. Wang, and A. C. Gossard, "Tunable, continuous-wave terahertz photomixer sources and applications," *Journal of Applied Physics*, vol. 109, no. 6, p. 061301, 2011. [Online]. Available: https://doi.org/10.1063/1.3552291

[21] C. W. Berry, M. R. Hashemi, and M. Jarrahi, "Generation of high power pulsed terahertz radiation using a plasmonic photoconductive emitter array with logarithmic spiral antennas," *Applied Physics Letters*, vol. 104, no. 8, p. 081122, 2014.

[22] A. Zangana, S. Al-Daffaie, O. Yilmazoglu, and F. Kueppers, "Graphene enhanced 2-d nanoelectrode for continuous wave terahertz photomixers," 09 2018.

[23] S.-H. Yang and M. Jarrahi, "Frequency-tunable continuous-wave terahertz sources based on gaas plasmonic photomixers," *Applied Physics Letters*, vol. 107, no. 13, p. 131111, 2015.

[24] Y. Mushiake, *Self-complementary antennas: principle of self-complementarity for constant impedance*. Springer Science & Business Media, 2012.

[25] D. M. Pozar, "Microwave engineering," *Wiley*, 2012.

[26] "Impedance matching network designer," https://home.sandiego.edu/~ekim/e194rfs01/jwmatcher/matcher2.html, 1997.

[27] J. B. Soole and H. Schumacher, "Ingaas metal-semiconductor-metal photodetectors for long wavelength optical communications," *IEEE journal of quantum electronics*, vol. 27, no. 3, pp. 737–752, 1991.

[28] P. J. Bevelacqua, "S-parameters. antenna theory," urlhttp://www.antenna-theory.com/definitions/sparameters.php, 2008-2015.

[29] A. Hoggard, L.-Y. Wang, L. Ma, Y. Fang, G. You, J. Olson, Z. Liu, W.-S. Chang, P. M. Ajayan, and S. Link, "Using the plasmon linewidth to calculate the time and efficiency of electron transfer between gold nanorods and graphene," *ACS Nano*, vol. 7, no. 12, pp. 11 209–11 217, 2013, pMID: 24266755. [Online]. Available: https://doi.org/10.1021/nn404985h

[30] X. Zhang, Y. Liu, S.-T. Lee, S. Yang, and Z. Kang, "Coupling surface plasmon resonance of gold nanoparticles with slow-photon-effect of tio 2 photonic crystals for synergistically enhanced photoelectrochemical water splitting," *Energy & Environmental Science*, vol. 7, no. 4, pp. 1409–1419, 2014.

[31] S. Lepeshov, A. Gorodetsky, A. Krasnok, E. Rafailov, and P. Belov, "Enhancement of terahertz photoconductive antenna operation by optical nanoantennas," *Laser & Photonics Reviews*, vol. 11, no. 1, p. 1600199, 2017.

[32] S. Al-Daffaie, O. Yilmazoglu, F. Kuppers, and H. L. Hartnagel, "Single nanowire photomixer for reliable and high frequency continuous wave terahertz generation," *2014 39th International Conference on Infrared, Millimeter, and Terahertz waves (IRMMW-THz)*, pp. 1–2, 2014.

[33] S. Al-Daffaie, O. Yilmazoglu, F. Küppers, and H. L. Hartnagel, "1-d and 2-d nanocontacts for reliable and efficient terahertz photomixers," *IEEE Transactions on Terahertz Science and Technology*, vol. 5, no. 3, pp. 398–405, May 2015.

[34] W. Zhao, X. Li, S. Gu, S. H. Kang, M. M. Nowak, and Y. Cao, "Field-based capacitance modeling for sub-65-nm on-chip interconnect," *IEEE Transactions on Electron Devices*, vol. 56, no. 9, pp. 1862–1872, Sep. 2009.

[35] B. Niesen, B. P. Rand, P. Van Dorpe, D. Cheyns, L. Tong, A. Dmitriev, and P. Heremans, "Plasmonic efficiency enhancement of high performance organic solar cells with a nanostructured rear electrode," *Advanced Energy Materials*, vol. 3, no. 2, pp. 145–150, 2013.

[36] M. Rycenga, C. M. Cobley, J. Zeng, W. Li, C. H. Moran, Q. Zhang, D. Qin, and Y. Xia, "Controlling the synthesis and assembly of silver nanostructures for plasmonic applications," *Chemical reviews*, vol. 111, no. 6, pp. 3669–3712, 2011.

[37] T. Kim, S. Kang, J. Heo, S. Cho, J. W. Kim, A. Choe, B. Walker, R. Shanker, H. Ko, and J. Y. Kim, "Nanoparticle-enhanced silver-nanowire plasmonic electrodes for high-performance organic optoelectronic devices," *Advanced Materials*, vol. 30, no. 28, p. 1800659, 2018.

[38] M. W. Knight, N. K. Grady, R. Bardhan, F. Hao, P. Nordlander, and N. J. Halas, "Nanoparticle-mediated coupling of light into a nanowire," *Nano Letters*, vol. 7, no. 8, pp. 2346–2350, 2007.

[39] D. Pan, H. Wei, Z. Jia, and H. Xu, "Mode conversion of propagating surface plasmons in nanophotonic networks induced by structural symmetry breaking," *Scientific reports*, vol. 4, p. 4993, 2014.

[40] F. Hao and P. Nordlander, "Plasmonic coupling between a metallic nanosphere and a thin metallic wire," *Applied physics letters*, vol. 89, no. 10, p. 103101, 2006.

[41] H. Choi, S.-J. Ko, Y. Choi, P. Joo, T. Kim, B. R. Lee, J.-W. Jung, H. J. Choi, M. Cha, J.-R. Jeong *et al.*, "Versatile surface plasmon resonance of carbon-dot-supported silver nanoparticles in polymer optoelectronic devices," *Nature Photonics*, vol. 7, no. 9, p. 732, 2013.

[42] Wikipedia contributors, "Stub (electronics) — Wikipedia, the free encyclopedia," 2019, [Online; accessed 15-October-2019]. [Online]. Available: https://en.wikipedia.org/w/index.php?title=Stub_(electronics)&oldid=909467491

List of Figures

List of Tables